EDGE ARTICLE

Check for updates

A host–guest strategy for converting the photodynamic agents from a singlet oxygen generator to a superoxide radical generator†

Kun-Xu Teng, Li-Ya Niu [ID] and Qing-Zheng Yang [ID] *

Type-I photosensitizers (PSs) generate cytotoxic oxygen radicals by electron transfer even in a hypoxic environment. Nevertheless, the preparation of type-I PSs remains a challenge due to the competition of triplet–triplet energy transfer with O_2 (type-II process). In this work, we report an effective strategy for converting the conventional type-II PS to a type-I PS by host–guest complexation. Electron-rich pillar[5]arenes are used as an electron donor and macrocyclic host to produce a host–guest complex with the traditional electron-deficient type-II PS, an iodide BODIPY-based guest. The host–guest complexation promotes intermolecular electron transfer from the pillar[5]arene moiety to BODIPY and then to O_2 by the type-I process upon light-irradiation, leading to efficient generation of the superoxide radical ($O_2^{-•}$). The results of anti-tumor studies indicate that this supramolecular PS demonstrates high photodynamic therapy efficacy even under hypoxic conditions. This work provides an efficient method to prepare type-I PSs from existing type-II PSs by using a supramolecular strategy.

Introduction

Photodynamic therapy (PDT) is a promising approach for cancer therapy that utilizes photosensitizers (PSs) in conjunction with molecular oxygen under light-irradiation to generate cytotoxic reactive oxygen species (ROS).[1–4] So far, most PSs produce singlet oxygen ($^1O_2$) through the type-II process by direct excitation energy transfer (EET) between the excited triplet state of the PS ($^3PS^*$) and O_2.[5–9] Unfortunately, PDT based on type-II PSs is highly O_2-dependent, thus the hypoxia of solid tumors would severely reduce the therapeutic efficacy in clinics.[10–12] In contrast, type-I PSs generate cytotoxic radicals through a cascade electron transfer (ET) reaction among $^3PS^*$, adjacent substrates and molecular oxygen.[13–15] Type-I PSs can lower the O_2 dependence and overcome the tumor hypoxia, thereby attracting increasing attention in recent years.[16–20]

However, the available type-I PSs are rarely reported and the design of type-I PSs remains a challenge.[21–24] The main reason for this is that the inefficient cascade ET reaction is always tough to compete with EET of $^3PS^*$ with oxygen (Fig. 1a).[25–28] Recently, our group has proposed that the EET process could be inhibited by decreasing the energy of $^3PS^*$ to below the requirement for sensitizing $^1O_2$, resulting in the blockage of the type-II process (Fig. 1b).[29] Although this strategy allows PSs to

exclusively generate ROS by the type-I process, it is hardly employed as universal guidance to prepare type-I PSs because of unpredictable triplet energy levels. Alternatively, another possible strategy to enhance the competitiveness of the type-I pathway is to increase the photoinduced electron transfer efficiency of PSs with substrates and oxygen (Fig. 1b).[30] Generally, in the type-I process, the PS first obtains an electron from nearby substrates (such as liposomes, NADH or amino acid) under light-irradiation to generate the anion radical ($PS^{-•}$),

Key Laboratory of Radiopharmaceuticals, Ministry of Education, College of Chemistry, Beijing Normal University, Beijing 100875, P. R. China. E-mail: qzyang@bnu.edu.cn

† Electronic supplementary information (ESI) available: Procedures for synthesis, characterization data, and supplementary figures. See https://doi.org/10.1039/d2sc01469f

Fig. 1 (a) The competition between excitation energy transfer and electron transfer in PDT. (b) The strategies for the design of type-I PSs: reported strategy (left) and proposed strategy in this work (right).

which further transfer the electron to molecular oxygen to produce $O_2^{-\bullet}$.[6] However, such cascade ET reactions are normally inefficient because PSs cannot effectively collide with nearby substrates.[31–33] Therefore, we anticipate that if we introduce electron-rich substrates into the current type-II PS and shorten the distance between the substrates and the PS, the ET efficiency would be enhanced to promote the type-I process.

Herein, we report a supramolecular strategy to efficiently convert the conventional type-II PS to a type-I PS by the host–guest interaction. The distance between the PS and the electron donor is shortened through the host–guest interaction, which promotes the electron transfer from the electron-rich host to the electron-deficient guest. As a proof-of-concept, iodide BODIPY (G), an electron-deficient and classic type-II PS with high efficiency of $^1O_2$ production, is used as a guest molecule and the electron-rich bispillar[5]arene (BP5A) is chosen as an electron donor and macrocyclic host (Fig. 2). The host–guest interactions between BP5A and G enable an effective electron transfer from BP5A to G by enhancing the electron cloud overlap between the electron-rich substrates and the PSs. Supramolecular polymers (HG) efficiently generate $O_2^{-\bullet}$ upon light irradiation, realizing the conversion of the type-II PS into a type-I PS. HG exhibits superior PDT performance even in a hypoxic environment of tumor cells.

Host–guest complexation of chromophore with macrocyclic host is a powerful method to modulate the properties of the guest.[34,35] The exploration of such systems through non-covalent synthesis is gathering tremendous interest due to its low cost and convenient construction manner beyond the molecular level.[36–39] Host–guest interactions have been employed to improve the fluorescence quantum yield of dyes,[40–45] inhibit aggregation-caused quenching,[46,47] design the supramolecular fluorescent probe,[48–50] and to enhance the generation capacity of $^1O_2$ for PDT.[51–53] However, converting type-II PSs to type-I PSs by the host–guest interaction has not been reported. To the best of our knowledge, the host–guest interaction is taken advantage of for the first time to successfully switch the sensitizing mechanism from the type-II to type-I reaction.

Results and discussion

We synthesized a classic type-II PS (G) as a guest molecule and a bispillar[5]arene as a host. The cyanoalkyl triazole moieties of

G have a strong affinity towards pillar[5]arenes.[54] The formation of a host–guest system is confirmed by ^1H NMR and 2D NOESY spectroscopy. ^1H NMR spectra of a mixture of BP5A and G suggested the formation of a supramolecular host–guest system (G $\subset$ BP5A), as evidenced by upfield shifts of methylene protons ($\Delta\delta_a = -3.06$ ppm, $\Delta\delta_b = -3.38$ ppm, $\Delta\delta_c = -2.92$ ppm, and $\Delta\delta_d = -2.14$ ppm, Fig. S1 and S2†). The proton signals were assigned on the basis of the ^1H–^1H COSY spectrum (Fig. S3†). The 2D NOESY spectrum showed clear correlations between methylene protons of G and aromatic and methyl protons of BP5A, further confirming the formation of this inclusion complex (Fig. S4†). In addition, the diffusion coefficients decreased from 8.461×10^{-10} to 1.810×10^{-10} m^2 s^{-1} as the concentration of BP5A and G increased from 5 mM to 50 mM, suggesting the formation of supramolecular polymers (Fig. S5†). We prepared the supramolecular PS of HG from BP5A and G by a microemulsion method (Fig. S6†). Scanning electron microscopy (SEM) revealed that nanoparticles were uniformly distributed with well-defined shape and size (Fig. 3a). The average hydrodynamic diameter of HG estimated by dynamic light scattering was 59.3 ± 3.3 nm (Fig. 3b and S7†). HG absorbs at 665 nm and emits at 720 nm in water, which is slightly redshifted compared to G in DMF (Fig. 3c and S10†). HG has excellent stability and the supramolecular polymer based on the host–guest interaction is crucial for the preparation of its nanoparticles with a well-defined size and morphology (Fig. S8 and S9†).
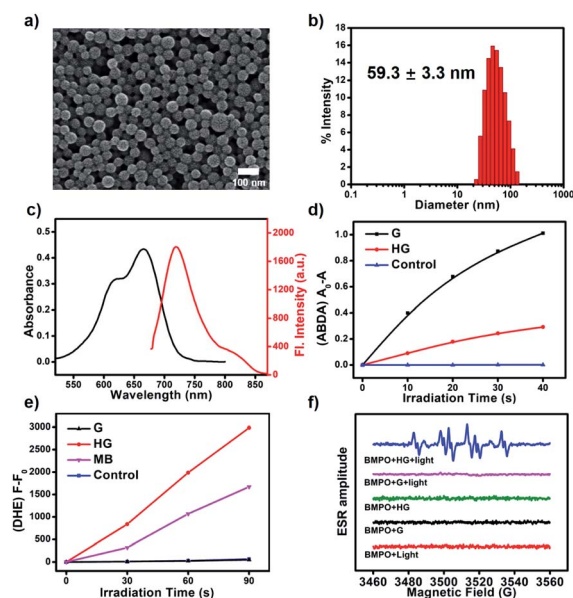

Fig. 3 (a) SEM image and (b) DLS of HG. (c) The absorption and fluorescence spectra of HG (10 μM) dispersed in water. (d) Plots of ΔAbs (A_0-A) for ABDA at 378 nm upon light irradiation (660 nm, 20 mW cm^{-2}) for different time intervals in the presence of G or HG. (e) Plots of ΔF_l ($F-F_0$) for DHE at 580 nm upon light irradiation (660 nm, 20 mW cm^{-2}) for different time intervals in the presence of G, HG or MB. (f) ESR spectra to detect $O_2^{-\bullet}$ generated by G (0.5 mM) and HG (0.5 mM) under illumination, using BMPO (25 mM) as a spin trap.

Fig. 2 The fabrication of HG and photo-induced generation of ROS.

To verify our anticipation, the ROS generation abilities of G and HG are investigated. Dihydroethidium (DHE) and 9,10-anthracenediyl-bis(methylene)dimalonic acid (ABDA) are employed as the specific $O_2^{-\cdot}$ and $^1O_2$ indicator, respectively. G exhibits strong $^1O_2$ productivity but no $O_2^{-\cdot}$ generation, confirming that G is a typical type-II PS (Fig. 3d and e). By contrast, as shown in Fig. 3d, the $^1O_2$ generation rate of HG is markedly reduced compared with that of G (Fig. S11†), suggesting that the excitation energy transfer between excited G and molecular oxygen is supressed. More importantly, upon light-irradiation, the fluorescence of the DHE solution in the presence of HG increases significantly, indicating that HG generates $O_2^{-\cdot}$ efficiently (Fig. 3e and S12†). As shown in Fig. 3e, the rate of $O_2^{-\cdot}$ generated by the irradiation of HG is 1.8-fold that of methylene blue (MB) under the identical conditions. The total ROS generation of HG and G was further evaluated by using 2′,7′-dichlorodihydrofluorescein (DCFH), a fluorescent probe to detect overall ROS, including $^1O_2$ and $O_2^{-\cdot}$. As can be seen in Fig. S13,† HG generates ROS faster than G, indicating that the total ROS generation capacity of HG is enhanced. Furthermore, the photodegradation experiment of rhodamine B (RhB) was employed to study the ROS generation of HG. It is known that RhB can be degraded by both $O_2^{-\cdot}$ and $^1O_2$.[55] As shown in Fig. S14,† the absorption of RhB in the presence of HG significantly reduced at 550 nm upon light-irradiation, suggesting that HG efficiently generated ROS and led to the photodegradation of RhB. Then, ROS quenchers were used to explore what type ROS is generated by HG. With the addition of 1,4-benzoquinone, a specific $O_2^{-\cdot}$ quencher, the absorption of RhB remains almost unchanged upon irradiation under the identical conditions, suggesting that HG primarily generated $O_2^{-\cdot}$. By contrast, the photodegradation rate of RhB only decreases a little in the presence of NaN_3, a selective $^1O_2$ scavenger, further confirming that HG generated much less $^1O_2$ than $O_2^{-\cdot}$. The above results demonstrate that the traditional type-II PS is effectively transformed into a type-I PS through the supramolecular host–guest strategy.

Electron spin resonance (ESR) spectroscopy is further employed to confirm the $O_2^{-\cdot}$ generation by sensitization of HG with BMPO as a spin-trap agent for $O_2^{-\cdot}$ (Fig. 3f). Upon light-irradiation of HG and BMPO in aqueous solution, a characteristic paramagnetic adduct is observed and well matched with the $O_2^{-\cdot}$ signal, confirming the generation of $O_2^{-\cdot}$. No ESR signals are observed for G and BMPO in DMSO under the identical conditions. And we also encapsulated G within Pluronic F127 to form G aggregates as a control to rule out aggregation of G as the cause of this conversion from type-II to type-I. Negligible ROS is produced for the G aggregates, indicating that aggregation of G quenches the excited state rather than switching it to type-I mechanisms (Fig. S15†).

We speculate that the efficient photoinduced electron transfer from BP5A to G facilitated by the host–guest interaction played a vital role in generating $O_2^{-\cdot}$. To confirm the intermolecular electron transfer enhanced by the host–guest interaction, cyclic voltammetry is conducted to determine the oxidation potential (E^{ox}) of G and BP5A. As shown in Fig. 4a and b, E^{ox} of G and BP5A is +0.387 V and +0.273 (vs. Fc/Fc$^+$),

respectively. The highest occupied molecular orbital (HOMO) and lowest unoccupied molecular orbital (LUMO) energy levels of G and BP5A are estimated through E^{ox} and the UV-vis absorption spectrum (Table 1 and Fig. S16†). As shown in Fig. 4c, BP5A serves as an electron donor to transfer an electron to excited G to generate G$^{-\cdot}$, which further transfers an electron to molecular oxygen and produces $O_2^{-\cdot}$. To further confirm the occurrence of photoinduced electron transfer, we study the Stern–Volmer quenching of the emission of G with the electron-rich host BP5A. As shown in Fig. 4d, the emission of G is gradually quenched with the addition of BP5A. The Stern–Volmer plots (Fig. 4e) show a linear correlation between the amounts of BP5A and the $(I_0–I)/I$ ratio, indicating that the host BP5A quenches the excited state of G by electron transfer. The Stern–Volmer quenching constant, K_{sv}, is 33.2 M^{-1}.

The PDT activity of HG in vitro is evaluated under both normoxic and hypoxic conditions. The fluorescence imaging experiment indicates the uptake of HG by HeLa cells (Fig. S17†). The ROS probe (DCFH-DA) and $O_2^{-\cdot}$ probe (DHE) are respectively employed to detect the cellular ROS generation during
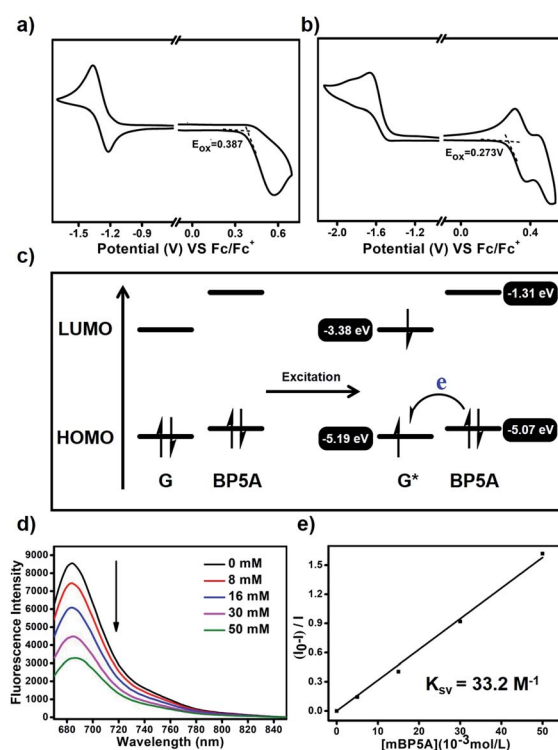

Fig. 4 Cyclic voltammogram of (a) G and (b) BP5A in DCM with 0.1 M $(n\text{-Bu})_4N^+PF_6^-$ as the supporting electrolyte, Ag/Ag$^+$ as the reference electrode, a glassy-carbon electrode as the working electrode and a Pt wire as the counter electrode; scan rate, 100 mV s^{-1}; Fc/Fc$^+$ was used as an external reference. (c) Schematic diagram of the electron transfer process between G and BP5A through HOMO and LUMO energy levels. (d) The emission spectra of G (1.0 × 10^{-5} M) at 25 °C in acetonitrile with increasing amounts of BP5A (0–50 mM) under excitation at 650 nm. (e) The Stern–Volmer plots for the fluorescence quenching of G by BP5A in acetonitrile at 25 °C (I_0 is the fluorescence intensity of G in the absence of BP5A and I is the fluorescence intensity in the presence of BP5A at the different concentrations ranging from 8 mM to 50 mM).

Table 1 Electrochemical potentials and energy levels of G and BP5A

Compd	E^{oxa} (V)	$E_g{}^b$ (eV)	HOMO^c (eV)	LUMO^d (eV)
G	+0.387	1.81	−5.19	−3.38
BP5A	+0.273	3.76	−5.07	−1.31

^{a} Oxidation potentials measured by cyclic voltammetry with ferrocene as the standard. ^{b} Band gap estimated from the UV-vis absorption spectrum. ^{c} Calculated from the oxidation potentials. ^{d} Deduced from the HOMO and E_g.

PDT in normoxic (21% O$_2$) and hypoxic environments (2% O$_2$). As shown in Fig. 5a, HeLa cells treated with HG and the probe DCFH-DA or DHE manifest obvious fluorescence signals of the products produced by the reaction of the probe with ROS after illumination in both normoxic and hypoxic environments, suggesting that the generation of ROS by HG is less dependent on the oxygen concentration. The cell counting kit-8 (CCK-8) assays are used to further evaluate the PDT effects of HG on HeLa cells. HG shows almost no dark toxicity in both normoxic and hypoxic environments (Fig. 5b). Under light-irradiation for 10 min, HG effectively kills HeLa cells even in a hypoxic environment. IC$_{50}$ is 4.7 μM under normoxia and 6.4 μM under hypoxia (Fig. 5c). A calcein-AM/PI assay is used to investigate the inhibition of tumor cells by HG (Fig. 5d). Viable cells were stained by using calcein-AM to emit fluorescence in the green

channel and apoptotic cells were stained by using PI to emit fluorescence in the red channel. HeLa cells treated with 4 μM HG show obvious fluorescence in the green and red channels after 660 nm light-irradiation, indicating partial cell death. When the HG concentration increases to 8 μM, all cells are dead. By contrast, HeLa cells without illumination only exhibit fluorescence in the green channel under identical conditions, indicating no cell death. Then, an annexin V-FITC/PI apoptosis detection kit is used to investigate the apoptotic cells (Fig. 5e). These results prove that HG effectively induces tumor cell apoptosis. We further investigate the PDT activity of HG in immunodeficient mouse models by using the subcutaneous tumor model of HeLa in the BALB/c mice. The fluorescence imaging experiment in mice indicates that HG can be enriched in the tumor position (Fig. S18†). And HG shows effective tumor inhibition with negligible systemic cytotoxicity (Fig. S19†).

Conclusions

In conclusion, we report for the first time efficient conversion of the traditional type-II PS to a type I PS using a supramolecular strategy by host–guest complexation between the type-II PS and pillar[5]arene. The host–guest interaction effectively shortens the intermolecular distance between the PS guest (G) and the electron donor (BP5A), which promotes the electron transfer

Fig. 5 (a) Detection of ROS and O$_2{}^{-•}$ in HeLa cells with DCFH-DA and DHE under normoxia (21% O$_2$) or hypoxia (2% O$_2$) conditions. The scale bar represents 50 μm. Cell viability of HeLa cells subjected to a range of HG concentrations in the (b) absence and (c) presence of light-irradiation (660 nm, 50 mW cm^{-2}) under normoxia or hypoxia conditions. (d) CLSM images of calcein AM/PI-stained HeLa cells. The scale bar represents 200 μm. (e) Apoptosis analysis of HeLa cells treated with HG at various doses (the parameter of CLSM: green channel: 500–550 nm, excited at 487 nm; red channel: 570–620 nm, excited at 562 nm; NIR channel: 663–738 nm, excited at 638 nm).

from the macrocyclic BP5A to electron-deficient G. HG efficiently produces $O_2^{-\cdot}$ by the type-I process upon light irradiation and exhibits excellent PDT performance even in a hypoxic environment. This simple, efficient and versatile strategy for converting the sensitizing mechanism from the type-II to type-I reaction may inspire the development of new photosensitizers for PDT of hypoxic solid tumors.

Ethical statement

Procedures related to animal experiments were implemented in compliance with the China Animal Management Regulations (2017 Edition), and were approved by the animal care committee of Beijing Normal University.

Data availability

Experimental procedures and data supporting the research, not presented in the main manuscript, is included in the ESI.†

Author contributions

Q.-Z. Yang proposed the concept and supervised the project. K.-X. Teng, L.-Y. Niu and Q.-Z. Yang designed the experiments. K.-X. Teng synthesized compounds and performed all experiments. K.-X. Teng, L.-Y. Niu and Q.-Z. Yang wrote the manuscript. All authors contributed to preparation of the manuscript.

Conflicts of interest

There are no conflicts to declare.

Acknowledgements

Notes and references

1 D. W. Felsher, *Nat. Rev. Cancer*, 2003, **3**, 375–380.
2 P. Agostinis, K. Berg, K. A. Cengel, T. H. Foster, A. W. Girotti, S. O. Gollnick, S. M. Hahn, M. R. Hamblin, A. Juzeniene, D. Kessel, M. Korbelik, J. Moan, P. Mroz, D. Nowis, J. Piette, B. C. Wilson and J. Golab, *Ca-Cancer J. Clin.*, 2011, **61**, 250–281.
3 V. N. Nguyen, Y. Yan, J. Zhao and J. Yoon, *Acc. Chem. Res.*, 2021, **54**, 207–220.
4 X. Zhao, J. Liu, J. Fan, H. Chao and X. Peng, *Chem. Soc. Rev.*, 2021, **50**, 4185–4219.
5 J. Wang, Q. Gong, L. Wang, E. Hao and L. Jiao, *J. Porphyrins Phthalocyanines*, 2020, **24**, 603–635.
6 A. P. Castano, T. N. Demidova and M. R. Hamblin, *Photodiagn. Photodyn. Ther.*, 2004, **1**, 279–293.
7 K.-X. Teng, L.-Y. Niu, Y.-F. Kang and Q.-Z. Yang, *Chem. Sci.*, 2020, **11**, 9703–9711.
8 J. Xie, Y. Wang, W. Choi, P. Jangili, Y. Ge, Y. Xu, J. Kang, L. Liu, B. Zhang, Z. Xie, J. He, N. Xie, G. Nie, H. Zhang and J. S. Kim, *Chem. Soc. Rev.*, 2021, **50**, 9152–9201.
9 B. Yuan, H. Wang, J.-F. Xu and X. Zhang, *ACS Appl. Mater. Interfaces*, 2020, **12**, 26982–26990.
10 Q. Chen, L. Feng, J. Liu, W. Zhu, Z. Dong, Y. Wu and Z. Liu, *Adv. Mater.*, 2016, **28**, 7129–7136.
11 W. Piao, K. Hanaoka, T. Fujisawa, S. Takeuchi, T. Komatsu, T. Ueno, T. Terai, T. Tahara, T. Nagano and Y. Urano, *J. Am. Chem. Soc.*, 2017, **139**, 13713–13719.
12 Z. Y. Liu, T. Y. Cao, Y. D. Xue, M. T. Li, M. S. Wu, J. W. Engle, Q. J. He, W. B. Cai, M. B. Lan and W. Zhang, *Angew. Chem., Int. Ed.*, 2020, **59**, 3711–3717.
13 L. B. Josefsen and R. W. Boyle, *Met.-Based Drugs*, 2008, **2008**, 276109.
14 Z. Zhou, J. Song, L. Nie and X. Chen, *Chem. Soc. Rev.*, 2016, **45**, 6597–6626.
15 H. Huang, S. Banerjee, K. Qiu, P. Zhang, O. Blacque, T. Malcomson, M. J. Paterson, G. J. Clarkson, M. Staniforth, V. G. Stavros, G. Gasser, H. Chao and P. J. Sadler, *Nat. Chem.*, 2019, **11**, 1041–1048.
16 X. Li, N. Kwon, T. Guo, Z. Liu and J. Yoon, *Angew. Chem., Int. Ed.*, 2018, **57**, 11522–11531.
17 Y. Y. Zhao, L. Zhang, Z. Chen, B. Y. Zheng, M. Ke, X. Li and J. D. Huang, *J. Am. Chem. Soc.*, 2021, **143**, 13980–13989.
18 Y. Wang, Y. Li, Z. Zhang, L. Wang, D. Wang and B. Z. Tang, *Adv. Mater.*, 2021, **33**, 2103748.
19 H. Yuan, Z. Han, Y. Chen, F. Qi, H. Fang, Z. Guo, S. Zhang and W. He, *Angew. Chem., Int. Ed.*, 2021, **60**, 8174–8181.
20 J. Sun, X. Cai, C. Wang, K. Du, W. Chen, F. Feng and S. Wang, *J. Am. Chem. Soc.*, 2021, **143**, 868–878.
21 M. Li, J. Xia, R. Tian, J. Wang, J. Fan, J. Du, S. Long, X. Song, J. W. Foley and X. Peng, *J. Am. Chem. Soc.*, 2018, **140**, 14851–14859.
22 V. N. Nguyen, S. Qi, S. Kim, N. Kwon, G. Kim, Y. Yim, S. Park and J. Yoon, *J. Am. Chem. Soc.*, 2019, **141**, 16243–16248.
23 Y. Zhu, Q. Wu, C. Chen, G. Yang, H. Cao, Y. Gao, L. Jiao, E. Hao and W. Zhang, *Sci. Chin. Mater.*, 2021, **64**, 3101–3113.
24 J. Li, Z. Zhuang, Z. Zhao and B. Z. Tang, *View*, 2022, **3**, 20200121.
25 H. Imahori, K. Tamaki, Y. Araki, Y. Sekiguchi, O. Ito, Y. Sakata and S. Fukuzumi, *J. Am. Chem. Soc.*, 2002, **124**, 5165–5174.
26 Q. Li, C. Huang, L. Liu, R. Hu and J. Qu, *Cytometry, Part A*, 2018, **93**, 997–1003.
27 Z. Zhuang, J. Dai, M. Yu, J. Li, P. Shen, R. Hu, X. Lou, Z. Zhao and B. Z. Tang, *Chem. Sci.*, 2020, **11**, 3405–3417.
28 Y. Z. Peng, G. C. Guo, S. Guo, L. H. Kong, T. B. Lu and Z. M. Zhang, *Angew. Chem., Int. Ed.*, 2021, **60**, 22062–22069.
29 K.-X. Teng, W.-K. Chen, L.-Y. Niu, W.-H. Fang, G. Cui and Q.-Z. Yang, *Angew. Chem., Int. Ed.*, 2021, **60**, 19912–19920.
30 H. Ding, H. Yu, Y. Dong, R. Tian, G. Huang, D. A. Boothman, B. D. Sumer and J. Gao, *J. Controlled Release*, 2011, **156**, 276–280.
31 G.-J. Zhao, J.-Y. Liu, L.-C. Zhou and K.-L. Han, *J. Phys. Chem. B*, 2007, **111**, 8940–8945.

32 S. Wang, D. Yu and L. Dai, *J. Am. Chem. Soc.*, 2011, **133**, 5182–5185.

33 D. Escudero, *Acc. Chem. Res.*, 2016, **49**, 1816–1824.

34 R. N. Dsouza, U. Pischel and W. M. Nau, *Chem. Rev.*, 2011, **111**, 7941–7980.

35 X. Li, S. Lee and J. Yoon, *Chem. Soc. Rev.*, 2018, **47**, 1174–1188.

36 S. Horike, S. Shimomura and S. Kitagawa, *Nat. Chem.*, 2009, **1**, 695–704.

37 D. S. Guo and Y. Liu, *Acc. Chem. Res.*, 2014, **47**, 1925–1934.

38 X. Ma and Y. L. Zhao, *Chem. Rev.*, 2015, **115**, 7794–7839.

39 X. Huang, T. Chen, N. Mu, H. W. Lam, C. Sun, L. Yue, Q. Cheng, C. Gao, Z. Yuan and R. Wang, *Acta Biomater.*, 2021, **131**, 483–492.

40 C. Fan, W. Wu, J. J. Chruma, J. Zhao and C. Yang, *J. Am. Chem. Soc.*, 2016, **138**, 15405–15412.

41 H. Wu, Y. Chen, X. Dai, P. Li, J. F. Stoddart and Y. Liu, *J. Am. Chem. Soc.*, 2019, **141**, 6583–6591.

42 M. Hao, G. Sun, M. Zuo, Z. Xu, Y. Chen, X.-Y. Hu and L. Wang, *Angew. Chem., Int. Ed.*, 2020, **59**, 10095–10100.

43 H. Wu, Y. Wang, L. O. Jones, W. Liu, B. Song, Y. Cui, K. Cai, L. Zhang, D. Shen, X.-Y. Chen, Y. Jiao, C. L. Stern, X. Li, G. C. Schatz and J. F. Stoddart, *J. Am. Chem. Soc.*, 2020, **142**, 16849–16860.

44 L. Cheng, K. Liu, Y. Duan, H. Duan, Y. Li, M. Gao and L. Cao, *CCS Chem*, 2020, **18**, 2749–2751.

45 X.-Y. Lou and Y.-W. Yang, *J. Am. Chem. Soc.*, 2021, **143**, 11976–11981.

46 B. Tang, W.-L. Li, Y. Chang, B. Yuan, Y. Wu, M.-T. Zhang, J.-F. Xu, J. Li and X. Zhang, *Angew. Chem., Int. Ed.*, 2019, **58**, 15526–15531.

47 B. Hua, C. Zhang, W. Zhou, L. Shao, Z. Wang, L. Wang, H. Zhu and F. Huang, *J. Am. Chem. Soc.*, 2020, **142**, 16557–16561.

48 E. A. Appel, X. J. Loh, S. T. Jones, F. Biedermann, C. A. Dreiss and O. A. Scherman, *J. Am. Chem. Soc.*, 2012, **134**, 11767–11773.

49 C. R. Benson, L. Kacenauskaite, K. L. VanDenburgh, W. Zhao, B. Qiao, T. Sadhukhan, M. Pink, J. Chen, S. Borgi, C.-H. Chen, B. J. Davis, Y. C. Simon, K. Raghavachari, B. W. Laursen and A. H. Flood, *Chem*, 2020, **6**, 1978–1997.

50 W.-C. Geng, Z. Ye, Z. Zheng, J. Gao, J.-J. Li, M. R. Shah, L. Xiao and D.-S. Guo, *Angew. Chem., Int. Ed.*, 2021, **60**, 19614–19619.

51 K. Yang, Z. Zhang, J. Du, W. Li and Z. Pei, *Chem. Commun.*, 2020, **56**, 5865–5876.

52 B. Yuan, H. Wu, H. Wang, B. Tang, J.-F. Xu and X. Zhang, *Angew. Chem. Inter. Ed.*, 2021, **60**, 706–710.

53 J. Chen, S. Li, Z. Wang, Y. Pan, J. Wei, S. Lu, Q.-W. Zhang, L.-H. Wang and R. Wang, *Chem. Sci.*, 2021, **12**, 7727–7734.

54 C. Li, K. Han, J. Li, Y. Zhang, W. Chen, Y. Yu and X. Jia, *Chem.–Eu. J.*, 2013, **19**, 11892–11897.

55 C. Chen, W. Ma and J. Zhao, *Chem. Soc. Rev.*, 2010, **39**, 4206–4219.